Desalination and Water Treatment
www.deswater.com

doi: 10.5004/dwt.2018.21927

110 (2018) 129–138
April

Morphological and structural characterization of nano-structured montmorillonite for separation process applications

Hadi Azimi[a,*], Majid Hayati-Ashtiani[b]

[a]*Department of English, Faculty of Letters and Human Sciences, Shahid Beheshti University, Iran, Tel. +98 21 7393 2324; email: ha_azimi@sbu.ac.ir*
[b]*Department of Chemical Engineering, Faculty of Engineering, University of Kashan, Iran, Tel. +98 31 5591 2424; email: hayati@kashanu.ac.ir*

Received 29 January 2017; Accepted 20 January 2018

ABSTRACT

Conducting the morphological and structural characterization of nano-structured montmorillonite is a crucial step of the separation process applications of this soft phyllosilicate group of minerals. In this study, the instrumental analyses as well as BJH (Barett–Joyner–Halenda) pore size distribution, screen (granulometric) analysis and swelling index (SI) were applied to the characterization of the samples. X-ray powder diffraction and X-ray fluorescence analysis, pH, screen analysis and swelling test showed that the Na-montmorillonite and Ca-montmorillonite bentonite types and the monovalent or divalent cations such as K^+, Na^+ or Ca^{2+} play a key role for the swelling properties of montmorillonite. Scanning electron microscopy and transmission electron microscopy were employed to carefully study the morphological characteristics of montmorillonites in samples No. 1 and No. 2. The surface morphology of sample No. 2 was foliated, fluffier and smoother than that of sample No. 1 with a clearer sheet structure having a rougher surface. The particles in sample No. 2 were larger in size and more strongly aggregated. In contrast, the particles in swelling sample No. 1 showed rather smaller aggregates and smoother surfaces with some sharp edges and tips. Sample No. 2 presented a wide particle size distribution (from 3 to 30 μm), while a more homogenous distribution was found in sample No. 1 (around 5 μm). BJH clearly showed the dominance of the mesopores in the sample containing nano-, meso- and micropores. The volume values of micro- and mesopores were put in the following order: sample No. 1 > sample No. 2.

Keywords: Montmorillonite; Bentonite; Swelling; Morphology; Nano-structure

1. Introduction

Bentonite is one of the best known and most commonly used industrial clays widely used in different industries such as animal and poultry feed pelletization, cat litter box, desiccates, herbicides, insecticides, pesticides, medicines, nanoclays, pharmaceuticals, plastics, seed growth, etc. [1]. Montmorillonite is a 2:1 layer nano-porous and nano-structured mineral consisting of an octahedral sheet sandwiched between two tetrahedral silica sheets (TOT) as shown in Fig. 1. Interlayer water and exchangeable cations exist between the montmorillonite layers and the chemical formula (idealized formula) of this mineral is $(Si_4)^{IV}(Al_{2-y}Mg_y)^{VI}O_{10}(OH)_2,yM^+.nH_2O$ [2]. Swelling of bentonite is mainly caused by the swelling of montmorillonite. A swelling montmorillonite mineral expands by soaking water into its interlayers [3]. The molecules of water have the tendency to be adsorbed on ions and clay surfaces. The physical state of a bentonite changes from an anhydrous solid to gel in a cat litter box because of the swelling of the montmorillonite as the most important and dominant mineral of bentonite. In fact, it is the montmorillonite which determines the swelling properties of bentonites.

* Corresponding author.

In this study, bentonites are categorized into Na-montmorillonite and Ca-montmorillonite types so that more accurate results can be achieved for any further generalization.

Swelling as a very important property of montmorillonite appears in two forms: crystalline or microscopic depending on the hydration of the exchangeable cations. It is a short-range layer interaction. The osmotic or macroscopic swelling is due to the difference of ion concentration in the pores (interlayer spaces and mesopores) and the solution [4–6]. Such a crystalline or microscopic swellings are much more complex since the multi-scale structure of montmorillonites and the intermolecular forces acting between layers, cations and water determine its structure at the macroscopic scale. The magnitudes of macroscopic swelling strongly depend on the clay mineralogy, the valence of cations, the cation exchange capacity and the structure at the atomic scale through the clay aggregate orientation and texture at the aggregate scale through the grain and pore distribution. At the osmotic or macroscopic, the swelling of the montmorillonite increases in the sample volume during the water adsorption process. Water penetrates the interlayer and forces them apart causing the clay to swell in crystalline swelling. Furthermore, there is some external surface water adsorption in which the water molecules interact with the surface by electrostatic (Coulomb) interactions, which are stronger than H bonds to the hexagonal network of oxygen atoms (Fig. 1) and the surface energy is important in developing a layer [7,8].

In osmotic swelling, the range of d-spacing distribution increases in (001) d-spacing values [9]. The basal spacing of a montmorillonite may significantly increase from 2.2 nm (upper limit of crystalline swelling) [10] up to several decades nanometers depending on water content by osmotic swelling in liquid water [11].

The swelling behavior of clay minerals has been studied in detail by many authors [12–16] and the relationship between cation mobility and swelling has already been investigated in montmorillonite [17–19]. More recently, several authors [20–23] have studied the swelling behaviour of Na-bentonite as a function of its smectite content, void ratio, initial water content, solute concentration and cations nature [24]. The interlayer cation nature affects the structure of the interlayer water thus influencing the cations mobility [25]. The relationship between swelling and hydration energy for interlayer cations has been studied [8,17,19] but the simultaneous effects of pH and swelling index along with the other necessary instrumental analysis such as XRF has not been considered yet. The nature and amount of interlayer cations strongly influences the interlayer space, characterized by X-ray diffraction (XRD) [25–30] but using other new methods such as swelling index and granulometric tests were not considered in their result discussion. The montmorillonite layers are aggregated in the case of calcium-montmorillonite or calcium-saturated dispersions and are delaminated in the case of sodium-montmorillonite or sodium-saturated dispersions. There are so many parameters which modify the montmorillonite layer lamination (association) in the case of ca-montmorillonite or delamination (dissociation) in the case of ca-montmorillonite [31]. The properties of the montmorillonite sheets, including size, structure and morphology [32–39] are the most important ones.

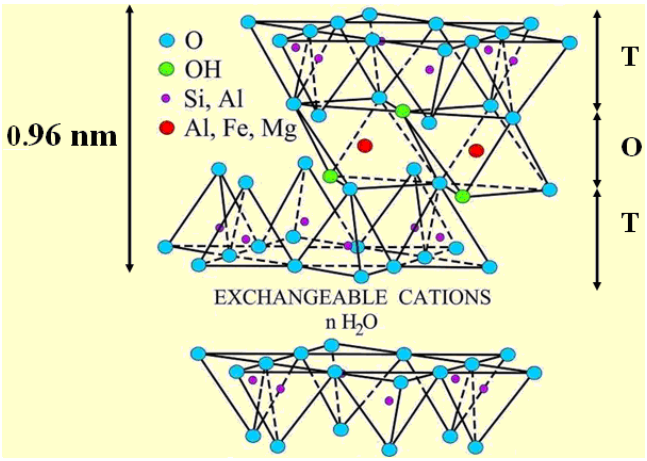

Fig. 1. Schematic representation of nano-montmorillonite structure [3].

Swelling is one of the physical properties of clay. The microstructure of the clays controls most of their physical properties such as swelling [40]. Electroscopic methods such as scanning electron microscopy (SEM) and transmission electron microscopy (TEM) are frequently employed to analyze the morphologies and structures of the swelling and non-swelling montmorillonites [41,42].

In the present paper, the morphology and structure of Na-montmorillonites and Ca-montmorillonites are studied through a combination of instrumental analyses such as SEM, TEM and BJH. The results of instrumental analyses were compared with the results of the volume change behavior of bentonite (swelling index). The novel insight provided in this study is a new approach through which it is possible to determine the swelling properties of bentonites through studying morphology and structure of montmorillonites along with SEM, TEM, BJH and their relations to swelling index.

2. Material and methods

2.1. Material and treatments

The clay minerals used in this study were bentonites. Two bentonites, namely sample No. 1 and sample No. 2 were used in their natural form. The sample name, origin and supplier of the bentonite samples are given in Table 1.

At the site, the air-dried chunks (<30 cm in diameter) were ground by primary and secondary (if necessary) jaw crushers to <5 cm. Then, less than 5 cm chunks were ground to 30–40 mm in diameter by a hammer crusher. At this stage, bentonites were sent into laboratory. At laboratory, samples

Table 1
Origin and supplier of bentonite samples

Sample name	Location of mine	Supplier
No. 1	Toroud, Semnan Province of Iran	Iran Mineral Processing Co., Seyed Abad Industrial Zone, Semnan, Iran
No. 2	Niagh, Gazvin Province of Iran	Kani Saze Jam Co., Gazvin, Iran

were first dried at the oven (Fan Azma Gostar V.2.1, Iran) over a night at 105°C ± 5°C and oven-dried samples were further ground by a laboratory jar and ball mill. Samples need more drying so that they can be more easily ground to smaller particles. The two prepared samples were powdered to less than 75 μm (U.S. Standard Sieve Mesh No. 200, Pars Sieve, Iran [ASTM E: 11]) and used for analyses.

2.2. pH effects

The pH of bentonite is a useful variable in determining the solubility of bentonite minerals including montmorillonite and the mobility of ions in bentonite [43]. The pH is a variable that controls the morphology by effecting the aggregation degree of negatively charged particles. For this test method, the air-dried bentonite samples were sieved through a No. 16 sieve (1 mm sieve mesh openings). 8 g of each sample was thoroughly mixed at least for 5 min in a vessel containing 100 mL distilled water. The pH was measured by a pH meter of Lutron, YK-2001 CT model. When making measurements with the pH electrode, the electrode was placed into the partially settled suspension to mitigate the suspension effect and the mixtures were approximately at room temperature.

2.3. X-ray fluorescence

X-ray fluorescence analysis is one of the most common techniques used for determining the compositional metals. Analyses were performed with an Oxford ED-2000 using XpertEase software.

2.4. X-ray powder diffraction

Mineralogical data of bentonite (natural and after treatment) were evaluated by X-ray powder diffraction (XRPD). Analyses were performed with a Philips PW 1800 diffractometer equipped with graphite secondary monochromator. Instrumental and measuring conditions were CuK_{α} radiation, 60 kV/40 mA, divergence and receiving slits of FINE, 0.020° 2θ step, 0.75 h step, using a time per step of 0.500 s. The XRPD pattern was collected from 2.010° to 60.000° (2θ).

2.5. Screen (granulometric) analysis

For screen analysis, 500 g of each bentonite sample were ground by a jar and ball mill for an hour, and the samples were passed through a U.S. Standard Sieve Mesh No. 16. Then, approximately 250 g of bentonite from each sample were dried (API, Section 4: BENTONITE) for 4 h at 110°C. Samples of approximately 100 g were weighed to the nearest 0.1 g and transferred to different dry standard sieve mesh numbers. It was shaken until no further material passed through each sieve. The residue was transferred to a watch glass weighed to the nearest 0.01 g and the glass plus residue was weighed to the nearest 0.01 g. The percentage was determined by the amount passing through the sieve from Eq. (1) reporting to the nearest %1:

$$\%\ \text{by weight through sieve} = \frac{W_1 - (W_3 - W_2)}{W_1} \times 100 \quad (1)$$

In Eq. (1), W_1 = sample weight, W_2 = watch glass weight, W_3 = watch glass weight plus residue.

2.6. Scanning electron microscopy

A Philips XL30 SEM was used to take photographs of the montmorillonites. SEM system works at 30 kV of electron accelerating maximum voltage and has LaB6 filament and maximum spot magnification of 80,000×. The sample was dispersed in ethanol prior to analysis using an ultrasonic bath for SEM/TEM morphological characterizations. Subsequently, a drop of the dispersion was poured to a holey carbon grid and the excess solution was blotted off. Samples were lightly gold-coated prior to put them on a holey carbon grid with a layer about 4–5 nm thick using a vacuum of 5×10^{-6} Pa (3.8×10^{-8} Torr) metal-coating process.

2.7. Transmission electron microscopy

TEM characterization of samples was performed using a Philips EM208S transmission electron microscope, operated at 100 kV acceleration voltages.

2.7.1. Specific surface measurements and pore size distribution

2.7.1.1. BET specific surface area measurement and BJH pore size distribution methods BET (Brunauer–Emmett–Teller) specific surface area and pore size distribution of original samples of Mesh No. 16 (ASTM E: 11) of bentonites were determined using the Quantachrome NOVA 2000e series volumetric gas adsorption instrument, which is a USA automated gas adsorption system using nitrogen. The determination is based on measuring the nitrogen adsorption. Experiments for adsorption isotherms were performed at 77.3 K and at the relative pressure up to $P/P_0 \sim 0.99$. Moisture and gases such as nitrogen and oxygen which were adsorbed on the solid surface or held in the open pores were removed under reduced pressure at 100°C for 8 h before measuring the specific surface area and pore size distribution. The pore size distribution of samples was calculated from desorption isotherms using the BJH (Barett–Joyner–Halenda) method.

2.7.1.2. Methylene blue specific surface area measurement Methylene blue (MB) chloride powder (Merck, Germany) was used in this study. According to the European standard (spot test), this procedure was followed by step by step [44]: (i) preparing the methylene blue solution by mixing 1.0 g of dry powder with 200 mL of deionized water; (ii) preparing the soil suspension by mixing 10 g of an oven-dried soil with 30 mL of deionized water; (iii) adding the methylene blue solution to the soil suspension in 0.5 mL increments; (iv) mixing the soil suspension for 1 min for each addition of MB; (v) removing a small drop of the suspension, and place it on Fisher brand filter paper Albet; (vi) determining the specific surface from the amount of MB required to reach the end point. When the unabsorbed methylene blue formed a permanent light blue halo around the soil aggregate spot, the "end point" was reached (i.e., the MB had replaced cations in the

double layer and had coated all the mineral surfaces). Eq. (2) shows the relationship between specific surface and MB:

$$\mathrm{SSA} = \frac{1}{319.87}\frac{1}{200}\left(0.5N\right)A_v A_{\mathrm{MB}}\frac{1}{10} \quad (2)$$

where N is the number of MB increments added to the soil suspension solution, A_v is Avogadro's number (6.02×10^{23}/mol), and A_{MB} is the area covered by one MB molecule (typically assumed to be 130 Å^2).

Adding 0.5 mL methylene blue solution in each step is low for clays with high specific surface area such as bentonite. So, 20 mL of methylene blue solution is added in each step and the suspension is stirred for 40 min in this research.

2.8. Swelling test

This test method covers an index (swell index) method that enables the evaluation of swelling properties of a clay mineral in reagent water for estimation of its usefulness for permeability. Swelling tests were carried out in accordance with ASTM D 5890-02. Powdered clay mineral is tested after drying to constant weight. The bentonite passing the 100 mesh standard sieve is used for testing after drying to constant weight at 105°C ± 5°C. Two-gram samples were gradually added in 0.1 g increments to 90 mL of reagent water in a 100-mL graduated cylinder. After 2 h from the last increment addition, it was inspected the hydrating bentonites column for trapped air or water separation in the column. The swell index (SI) values corresponding to the volume of swollen sample were recorded in millimeters after a minimum of 16-h hydration period from the last increment addition.

3. Results

3.1. X-ray diffraction

Fig. 2(a) (Ca-bentonites) and Fig. 2(b) (Na-bentonites) show the XRD patterns of the samples. Individual minerals (montmorillonites) were identified according to ASTM cards (Powder Diffraction File, Inorganic Phases). The XRD pattern of the natural clays of samples No. 1 and No. 2 showed the characteristic of d-spacing of 4.45, 2.54 and 1.49 Å. So, the samples are bentonites. The peak at 4.45 Å further implies the 2:1 montmorillonite. The XRD pattern also indicates quartz (4.24 Å) for both samples. XRD pattern of sample No. 1 XRD pattern indicated basanite (3.01 Å), cristobalite (4.05 Å), feldspar, that is, albite, (2.12 Å) and halite (2.82 Å). Montmorillonites have d-spacings of 15.17 and 14.40 Å, respectively.

The XRD results are in agreement with the SEM image. SEM identifies the surface morphology and size of the montmorillonite.

3.2. Screen (granulometric) analysis

Screen (granulometric) analysis is a good method to compare finer portions of porous clayey intra- and interparticles and coarser portions of non-porous non-clayey particles of bentonites. The porous particles of a bentonite with finer sizes have the major swelling effect of a bentonite. The result of screen analysis shows that the particle distribution is not homogeneous since the samples have different grain sizes (Table 2). Table 2 indicates the content of finer porous parts of sample No. 1 (passing mesh No. 400 or finer than 36 μm) is more than that of sample No. 2 and the coarser non-porous parts are observed for sample No. 2 (less than Mesh No. 16 [1,000 μm] but greater than mesh No. 120 [125 μm]). So, the diffusion of water molecules must be more in finer porous content layers of bentonite (montmorillonite) sample No. 1 (Na-montmorillonite) which means more swelling properties.

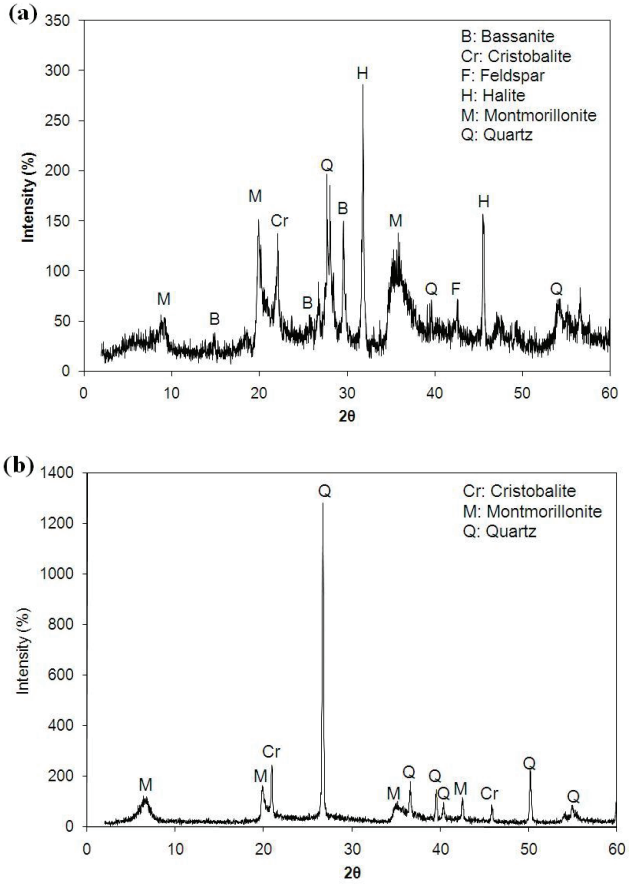

Fig. 2. X-ray diffraction patterns of (a) sample No. 1 and (b) sample No. 2.

Table 2
Screen (granulometric) analysis of particles of studied bentonite samples

Mesh No. (μm)	No. 1	No. 2
–16 + 120 (–1,000 + 125)	7	46.32
–120 + 200 (–125 + 75)	29.53	24.24
–200 + 325 (–75 + 40)	23.17	12.67
–325 + 400 (–40 + 36)	10.11	1.21
–400 (–36)	29.32	13.25
Total weight	99.13	97.8

3.3. X-ray fluorescence

Bentonite chemical analysis (XRF) is reported in Table 3. The high proportion of SiO_2 and Al_2O_3 demonstrates the presence of montmorillonite. The presence of Na_2O, CaO, MgO, FeO or Fe_2O_3, K_2O, P_2O_5, SO_3 and TiO_2 can also be observed. Small amounts of P, S and Ti from phosphor, sulphur and titanium oxide also exist without changing the swelling properties of clay. Na content indicates variable cation amount, which is defined along with pH, screen analysis and swelling index, and the type of Na- and Ca-montmorillonites. The amount of Na_2O (2.2 wt%) in the sample No. 1 is higher than that of 1.4 wt% of Na_2O in sample No. 2 but the amount of CaO (0.2 wt%) in sample No. 1 is lower than that of 1.7 wt% of CaO in sample No. 2. It is obvious that Na-montmorillonites equivalents have a greater amount of Na_2O than that of Ca-montmorillonites.

3.4. Swelling test

The results show swell indices of samples No. 1 and No. 2 are 24 and 4 mL, respectively. There is a direct relationship between swell index, MB specific surface area measurement and pore size distribution. Swelling strongly depends on the nature of the interlayer cations and the interlayer space depends on the nature of the interlayer cations. These parameters are with respect to the montmorillonite content of a bentonite which means they are dominated by the character of the only very fine end of dry screen (granulometric) analysis and they are essential to predict the type and properties of montmorillonites.

3.5. Morphology of montmorillonite with scanning electron microscopy

Generally, montmorillonite particles are heterogeneous and irregular, with sizes ranging from several μm to about 100 μm, with most particles measuring about 10 μm. Thus, SEM is a good method for determining the morphology of the montmorillonite aggregates and surface structures. The particle surfaces display a feathery appearance, reflecting the presence of montmorillonite. Montmorillonite is highly porous in nature and shows large agglomerates of very fine particles. The montmorillonite looks like a wavy, fuzzy and crumpled sheets varying in thickness. This type of partially flocculated arrangement of particles is common in montmorillonite samples. No morphological similarity exists because of the penetration of certain molecules into the interlayer spaces of montmorillonite sheets.

The SEM images of montmorillonite samples are shown in Figs. 3(a) and (d) (magnification 5,000×), in Figs. 3(b) and (e) (magnification 10,000×), and in Figs. 3(c) and (f) (magnification 20,000×). The surface morphology of both samples indicates a layered structure of montmorillonite. The individual particles, most of them having clearly recognizable contours, are irregular platelets but tend to form some thick and large agglomerates, especially in the sample No. 2.

The SEM photographs of sample No. 1 (Figs. 3(a)–(c)) highlight the shape of swelling montmorillonite as a spongy (porous) appearance with irregular structure and open voids in the surface morphology, where the surface is unsmooth. The surface morphology of sample No. 2 (Fig. 3(f)) is foliated, fluffier and smoother than that of sample No. 1 (Fig. 3(c)) with a clearer sheet structure having a rougher surface. The particles of samples No. 2 are larger in size and more strongly aggregated in shape. In contrast, the particles of swelling samples No. 1 show smaller aggregates and smoother surfaces, and sharp edges and tips (Figs. 3(c) and (f)).

A larger magnification view of the above photograph can be seen in Figs. 3(b) and (c) which show the presence of a fine particulate arrangement of the constituents. A detailed observation of all samples revealed that sample No. 2 presents a wide particle size distribution (from 3 to 30 μm), while in sample No. 1 a more homogenous distribution is found (around 5 μm). This fact indicates a different agglomeration state of sample No. 1 compared with sample No. 2, as it is also pointed out by the pore size distribution measurements.

Table 3
XRF results of studied bentonite samples

Analyte (%wt)	No. 1	No. 2
Na_2O	2.2	1.4
CaO	0.2	1.7
SiO_2	64.4	74.2
Al_2O_3	14.3	16
MgO	3.6	3.8
P_2O_5	0.6	0.5
SO_3	0.55	0.5
Cl	5.5	–
K_2O	0.2	0.3
TiO_2	0.5	0.1
TFeO[a]	2	0.8
H_2O	2.5	1.4

[a]TFeO = FeO + Fe_2O_3.

3.6. Transmission electron microscopy

Fig. 4 shows the TEM images of montmorillonite samples No. 1 and No. 2. The TEM of the nano-montmorillonite shows the morphology of nano-montmorillonite nano-platelet which has a wire or fiber structure. It also shows that the stacks of multilayers of samples No. 1 and No. 2 became thin and dispersive, which showed the dispersion morphology of montmorillonite nano-platelets.

3.7. Specific surface area measurement and pore size distribution

3.7.1. BET, MB specific surface area and BJH pore size distribution methods

The gas adsorption technique defines specific surface area, size and distribution of the pores. The amount of gas needed to form a monolayer N_2 on a solid surface can be determined by measuring the volume of gas adsorbed when pressure was increased in small amount at a constant temperature. These analyses were performed using a BET method.

BET and MB surface area measurements were carefully applied to samples No. 1 and No. 2 as illustrated in Table 4.

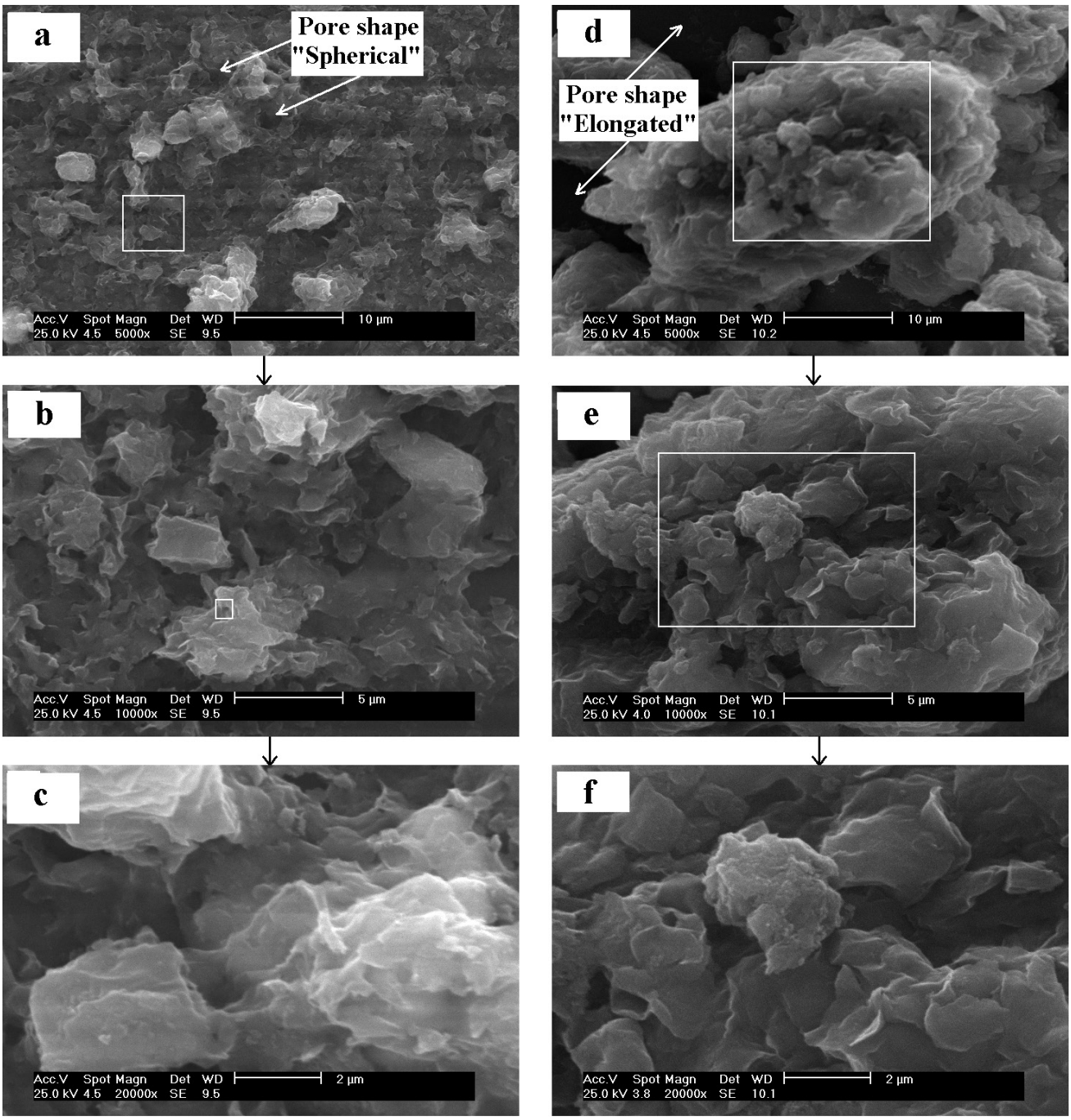

Fig. 3. SEM photographs of Na-montmorillonite (sample No. 1) and Ca-montmorillonite (sample No. 2) at increasing magnifications: (a) No. 1 (5,000×), (b) No. 1 (10,000×), (c) No. 1 (20,000×), (d) No. 1 (5,000×), (e) No. 1 (10,000×) and (f) No. 1 (20,000×).

According to the data presented for montmorillonite clay [44,46], the N_2 adsorption method is not conclusive for determining the specific area. These authors point out that nitrogen adsorption is performed under dry conditions in which the montmorillonite layers are tightly bound together. Thus, the molecules from the selected gas cannot penetrate into the interlayer surfaces and the amount of N_2 adsorbed measures only the external surface areas of montmorillonites. This can be observed in the natural clay in this work (Table 2), where the MB surface area is much greater than the area determined by N_2 adsorption, due to surface area between the montmorillonite layers that is enabled by delaminating in liquid by MB. For sample No. 2, the measured surface area was smaller than that of sample No. 1, probably due to the much smaller number of pores in the nano-montmorillonite.

The BJH method was applied for the pore size distribution from adsorption–desorption data. Nitrogen isotherms (Fig. 5) showed the type II isotherm in the BDDT (Brunauer, Demming, Demming and Teller) classification. This S-shaped isotherm type is frequently found in non-porous solids or in

those with pores larger than micropores. Fig. 5 shows desorption of N_2 isotherms, which practically coincide with those of adsorption, thus indicating the hysteresis characteristic of an adsorption process.

3.7.2. Structural pore studies

The average pore diameters and BJH pore volumes were shown in Table 4. The International Union of Pure and Applied Chemistry – IUPAC [45] classifies the diameters of pores wider than 50 nm as macropores, pores from 2 to 50 nm width as mesopores, and those with less than 2 nm as micropores. The N_2 sorption method also provides the basis for determining the pore distribution behavior of adsorbents. However, the BET method uses nitrogen, a very small molecule to obtain pore distribution. Therefore, it tends to be more suitable for the analysis of microporous materials. Fig. 6 shows the predominance of mesopores for both samples.

Using Fig. 5, the mesopores (V_{mes}) and micropores (V_{mi}) volumes were obtained by reading the adsorbed volumes (V_{ads}) in $P/P_0 = 0.10$ and 0.95 expressed by Eqs. (3) and (4):

$$V_{mi} = V_{ads\ (P/P_0 = 0.10)} \tag{3}$$

$$V_{mes} = V_{ads\ (P/P_0 = 0.95)} - V_{ads\ (P/P_0 = 0.1)} \tag{4}$$

Here, P_0 and P are the vapor pressure of the bulk liquid nitrogen and equilibrium pressure of desorption at the liquid nitrogen temperature (~77 K). The result of V_{mi} and V_{mes} were calculated with respect to Fig. 5 and summarized in Table 4. The results showed that the surface area, meso- and micropore volume values were arranged in the following sequence: sample No. 1 > sample No. 2.

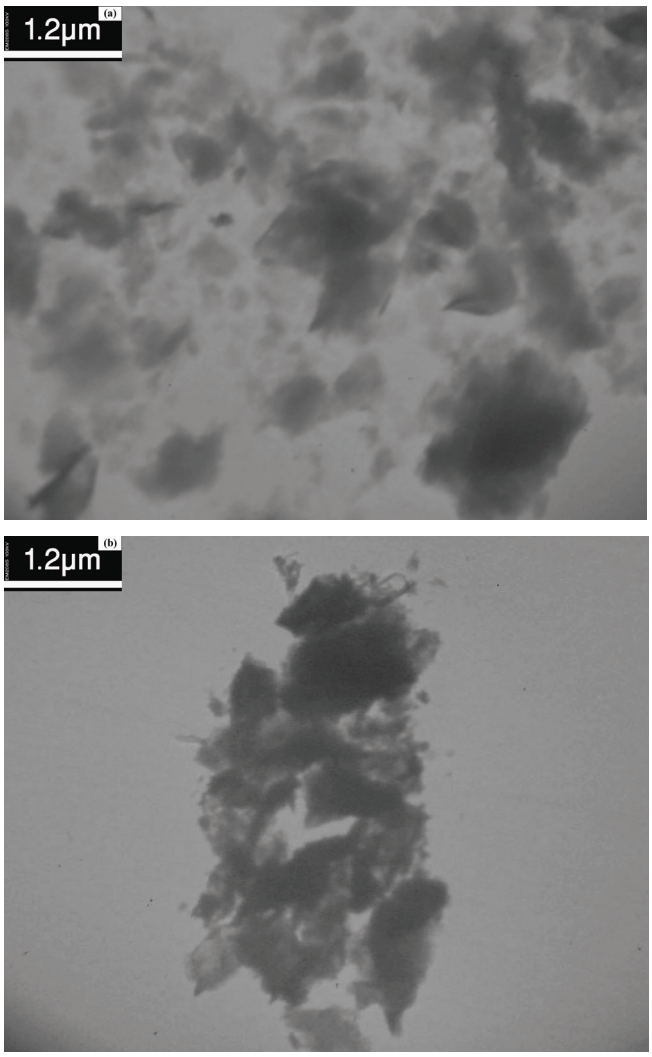

Fig. 4. TEM images of samples (a) No. 1 and (b) No. 2.

Table 4
Structural characteristics of natural nano-montmorillonite

Samples	No. 1	No. 2
S_{BET} (m^2/g)	51	9
S_{MB} (m^2/g)	832	563
Pore volume (mL/g)	0.078	0.075
V_{mi} (mL/g)	13.5	8.3
V_{mes} (mL/g)	45	28.5
d_{Pore} average (nm)	1.98	2.2

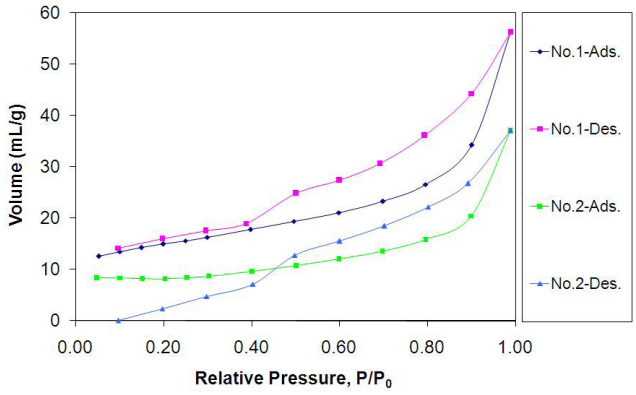

Fig. 5. Nitrogen adsorption–desorption isotherms of bentonites of samples No. 1 and No. 2.

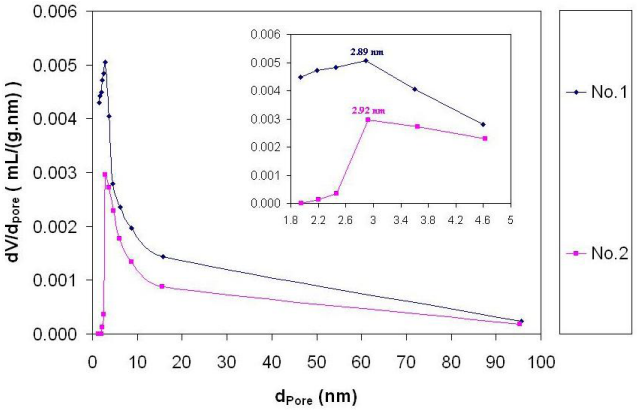

Fig. 6. Derivative pore volume distribution curve of bentonites of samples No. 1 and No. 2.

The volumes of meso- and micropores (V_{mi+mes}) of samples No. 1 and No. 2 were reported as 58.5 and 36.8 mL/g, respectively. Approximately 23% of the volume of adsorbed nitrogen at $P/P_0 = 0.1$ was related to the micropores of samples No. 1 and No. 2.

As an example, the SEM photographs of sample No. 1 (magnitude 80,000×) are shown in Figs. 3(c) and (f). In SEM photographs Figs. 3(c) and (f), the meso- and macroporous structures were observed. As the SEM photographs show the difference in micropore structure was clearly found between both montmorillonites. Fig. 3(a) indicated that the shapes of pores in general were irregular, approximately spherical, mostly discrete but sometimes interconnected. There are a few relatively large voids. The larger microstructure in typical montmorillonite layers was found in sample No. 1 (Na-bentonite) with the most montmorillonite content (Table 2) and is clearly seen in Figs. 3(a) and (d).

4. Discussion

XRD results indicate that the subtraction of the thickness of the 2:1 layer of 9.60 Å yields an interlayer separation of 5.57 and 4.8 Å in samples No. 1 and No. 2, respectively. The increase in d-spacing is due to the cation exchange which results in an expansion in the interlayer spacing. The amount of the exchanged cations in sample No. 1 is more than that of sample No. 2 which is predicted to have lower swelling properties. The results of XRD also indicate that the sample with more SiO_2 content (sample No. 2) is the bentonite with some smaller montmorillonite content (Table 2). The chemical and XRD analyses (Table 3 and Fig. 2) give the evidence on bentonite sample quality from the viewpoint of the montmorillonite and impurities content. Meanwhile, the XRD results show that the basal spacing of sample No. 1 is higher than that of sample No. 2. It means that the amount of interlayer cations and water molecules in sample No. 1 is higher than that of sample 2. The pH results are useful in determining the solubility of minerals and the exchanging of interlayer and loosely surface bonded cations such as Na^+, Ca^{2+}, K^+, etc. Sample No. 1 has the highest pH and swell index comparing with sample No. 2 which leads to the highest interlayer cations mobility since the water molecules entering the interlayer cations have the capability of hydrating the cations. When, as a result of water molecules adsorption, the interlayer space increases, the interaction between the clay layer and the cations decreases; therefore, the cation becomes more mobile and the cations enter the solution. Consequently, the released cations are hydrolyzed and they increase the pH. Salles et al. [47] and Douillard et al. [8] suggest some cations such as Na^+ and K^+ are preferentially hydrated in the interlayer space and then, entering the solution, in contrast with other monovalent cations. pH of samples No. 1 and No. 2 is 7.9 and 7.7, respectively. Both samples are alkaline but the alkalinity of sample No. 1 is higher than that of the other one. The higher pH of sample No. 1 indicates that it has more soluble mineral and mobilized cations to be hydrolyzed. Therefore, sample No. 1 should have more swelling properties as it is in agreement with the result of swelling index experiments. In addition to XRD results which approved the bentonites and the presence of montmorillonite, bentonite chemical analysis (XRF) (Table 3) indicates a high proportion of SiO_2 and Al_2O_3 which demonstrates the presence of montmorillonite. The amount of Na_2O is 2.2 wt% in sample No. 1 which is higher than that of 1.4 wt% of Na_2O in sample No. 2 but the amount of CaO is 0.2 wt% in sample No. 1 which is lower than that of 1.7 wt% of CaO in sample No. 2. The Na content indicates different amounts of cations which define along with pH, and swelling index, the type of Na-montmorillonite (sample 1) and Ca-montmorillonite (sample 2). When Na-montmorillonite soaks in the water, a hydration layer surrounds the Na^+ cation speeding the interaction between the cations and the clay layers. So, the interlayer cations become more mobile compared with Na-montmorillonite solids or hydrated Ca-montmorillonite. This conclusion is confirmed with the result of swelling index experiments and the swelling index of sample 1 is 24 mL while the swelling index of sample 2 is only 4 which is in agreement with other studies [48,49]. Furthermore, the amount of metal oxides from XRF and the pH results support the conclusion that Na-montmorillonite sample 1 has more soluble interlayer and the layer cations which increase the swelling effects, thus playing the key role in the adsorption of metals in the separation processes. Screen (granulometric) analysis results of samples indicate that a large content of expandable montmorillonite in bentonites is responsible for the swelling properties of these materials.

SEM reveals that the larger aggregate sizes of sample No. 2 is due to Ca^{2+} cations acting as functional groups and able to aggregate bentonite particles. As shown in Fig. 3, the montmorillonite of sample No. 1 (Fig. 3(a)) shows numerous internal channels compared with sample No. 2 (Fig. 3(d)). These frameworks are convenient for more water molecules to be adsorbed on the montmorillonite of sample No. 1.

It can be seen from Fig. 3 that sample No. 1 shows a small particle and porous surface. The incorporation of Na^+ can form large particles and numerous cavities, which may be convenient for the penetration of adsorbed molecules into the galleries of swelling montmorillonite and may result in an increase in the adsorption capacity in comparison with sample No. 2.

The surface morphology of Na-montmorillonite (sample No. 1) is different from that of Ca-montmorillonite (sample No. 2). The Na-bentonite appears as corn flake–shaped crystals with fluffy appearance revealing its extremely fine platy structure. Ca-montmorillonite is smoother and more aggregated. This smooth and aggregated appearance probably occurs due to the change in the surface charge of the particle because of amorphous substitution.

The increase of the montmorillonite content in Ca-montmorillonite or Na-montmorillonite is accomplished by formation of more microstructures. The sample with larger amount of Ca-montmorillonite (sample No. 2) indicates larger grain size of montmorillonite aggregates relative to Na-montmorillonite (sample No. 1). The increase of the montmorillonite content contributes to uniform, less permeable and more swellable microstructures. The comparison of microstructures in montmorillonite samples with different montmorillonite content (according to screen fine particle analysis samples No. 1 is richer on montmorillonite than that of sample No. 2) either Ca- or Na-form shows that Na-montmorillonite is more aggregated opposite to Ca-montmorillonite. This can be explained by higher swelling index of Na-montmorillonite (sample No. 1) particles

forming closely arranged microstructures compared with that formed in Ca-montmorillonite (sample No. 2) with lower water adsorption (lower swelling index) characteristics. The microstructures of montmorillonite particles in Ca-montmorillonite (Figs. 3(d)–(f)) is characterized by large amounts of leaves with elongated open-air voids having small interfacial zones and mutual bonds. In contrast, the microstructure of Na-bentonite (Figs. 3(a)–(c)) seems to contain a large volume of small leaflets with approximately spherical open-air voids placed very closely to each other, and thus creating compact layers of montmorillonite particles with large uniformity of the formed aggregates. The Na-open-air voids and Ca-open-air voids create different microstructures with comparable particle sizes as it was discussed.

TEM results are in agreement with SEM results. TEM observations (Figs. 4(a) and (b)) showed that submicron-sized flaky and plate-like particles morphology of montmorillonite are mainly the aggregation of almost rounded particles. Moreover, a higher porosity and a greater volume of mesopores could be observed in these clays. This result demonstrates the relevance of N_2 adsorption for assessing the pore characteristics of the adsorbent.

5. Conclusion

This research demonstrates the morphological and structural properties of two different types of bentonites and a new insight has been developed to determine the swelling of the interlayer cations and applied to study in the case of Na and Ca type montmorillonites. The different behavior patterns of both samples observed depend on the nature and the amount of the cations. Small cations (such as Na^+) showed a significant variation of the swelling and mobility together as a function of the pH confirmed with XRF and XRPD results. The XRPD reveals the bentonite and presence of montmorillonite but it does not clearly reveal the character of the formed microstructure and swelling characteristics of individual bentonite types. SEM along with BJH pore size distribution measurements clearly reveals the formed microstructure, the differences and similarities of particular samples. The properties of tested samples No. 1 and No. 2 are shown. Sample No. 2 (Ca-montmorillonite) shows the lower swelling capacity. This was confirmed by lower BET and real MB specific surface areas (9 and 563 m^2/g, respectively), mean pore size distribution (2.2 nm), and lower montmorillonite content as well.

This study has examined and uncovered the differences in various morphological and structural bentonites type behaviors.

References

[1] H.H. Murray, Applied Clay Mineralogy: Occurrences, Processing and Application of Kaolins, Bentonites, Palygorskite-Sepiolite, and Common Clays, Elsevier B.V., UK, 2007.

[2] F. Bergaya, B.K.G. Theng, G. Lagaly, Handbook of Clay Science, Elsevier, Amsterdam, 2006.

[3] F. Wypych, K.G. Satyanarayana, Clay Surfaces: Fundamentals and Applications, Elsevier Academic Press, UK, 2004.

[4] E. Ferrage, B. Lanson, B.A. Sakharov, V.A. Drits, Investigation of smectite hydration properties by modeling experimental X-ray diffraction patterns: Part I. Montmorillonite hydration properties, Am. Mineral., 90 (2005) 1358–1374.

[5] F. Salles, I. Beurroies, O. Bildstein, M. Jullien, J. Raynal, R. Denoyel, H. Van Damme, A calorimetric study of mesoscopic swelling and hydration sequence in solid Na-montmorillonite, Appl. Clay Sci., 39 (2008) 186–201.

[6] E. Ferrage, C.A. Kirk, G. Cressey, J. Cuadros, Dehydration of Ca-montmorillonite at the crystal scale. Part 2. Mechanisms and kinetics, Am. Mineral., 92 (2007) 1007–1017.

[7] B. Rotenberg, J.P. Morel, V. Marry, P. Turq, N. Morel-Desrosiers, On the driving force of cation exchange in clays: insights from combined microcalorimetry experiments and molecular simulation, Geochim. Cosmochim. Acta, 73 (2009) 4034–4044.

[8] J.M. Douillard, F. Salles, S. Devautour-Vinot, A. Manteghetti, M. Henry, Study of the surface energy of montmorillonite using PACHA formalism, J. Colloid Interface Sci., 306 (2007) 175–182.

[9] K. Norrish, The swelling of montmorillonite, Discuss. Faraday Soc., 18 (1954) 120–134.

[10] G. Lagaly, R. Fahn, Ullmann's Encyclopedia of Technical Chemistry, Verlag Chemie, Weinheim, 1993.

[11] Y.F. Xu, H. Matsuoka, D.A. Sun, Swelling characteristics of fractal-textured bentonite and its mixtures, Appl. Clay Sci., 22 (2003) 197–209.

[12] M. Hayati-Ashtiani, S.H. Jazayeri, M. Gannadi, A. Nozad, Experimental characterizations and swelling studies of natural and activated bentonites with their commercial applications, J. Chem. Eng. Jpn., 44 (2011) 67–77.

[13] P.F. Luckham, S. Rossi, The colloidal and rheological properties of bentonite suspensions, Adv. Colloid Interface Sci., 82 (1999) 43–92.

[14] H. Van Olphen, An Introduction to Clay Colloid Chemistry, John Wiley & Sons, New York, 1997.

[15] S.L. Swartzen-Allen, E. Matijevic, Surface and colloid chemistry of clays, Chem. Rev., 74 (1974) 385–400.

[16] R.J. Hunter, Foundations of Colloid Science, Oxford University Press, New York, 1986.

[17] F. Salles, O. Bildstein, J.M. Douillard, M. Jullien, J. Raynal, H. Van Damme, On the cation dependence of interlamellar and interparticular water and swelling in smectite clays, Langmuir, 26 (2010) 5028–5037.

[18] I. Bérend, L.M. Cases, M. François, J.P. Uriot, L. Michot, A. Masion, F. Thomas, Mechanism of adsorption and desorption of water vapor by homoionic montmorillonite: 3. The Mg^{2+}, Ca^{2+}, Sr^{2+} and Ba^{2+} exchanged forms, Clay Clay Miner., 43 (1995) 324–336.

[19] F. Salles, J.M. Douillard, R. Denoyel, O. Bildstein, M. Jullien, I. Beurroies, H. Van Damme, Hydration sequence of swelling clays: evolution of specific surface area and hydration energy, J. Colloid Interface Sci., 333 (2009) 510–522.

[20] H. Komine, N. Ogata, Experimental study on swelling characteristics of compacted bentonite, Can. Geotech. J., 31 (1994) 478–490.

[21] H. Komine, N. Ogata, Prediction for swelling characteristics of compacted bentonite, Can. Geotech. J., 33 (1996) 11–22.

[22] H. Komine, N. Ogata, Experimental study on swelling characteristics of sand-bentonite mixture for nuclear waste disposal, Soils Found., 39 (1999) 83–97.

[23] H. Komine, Simplified evaluation for swelling characteristics of bentonites, Eng. Geol., 71 (2004) 265–279.

[24] S. Tripathy, A. Sridharan, T. Schanz, Swelling pressures of compacted bentonites from diffuse double layer theory, Can. Geotech. J., 41 (2004) 437–450.

[25] C. Fourdrin, H. Aarachi, C. Latrille, S. Esnouf, F. Bergaya, S. Le Caer, Water radiolysis in exchanged-montmorillonites: the H_2 production mechanisms, Environ. Sci. Technol., 47 (2013) 9530–9537.

[26] M. Segad, B. Jonsson, T. Akesson, B. Cabane, Ca/Na montmorillonite: structure, forces and swelling properties, Langmuir, 26 (2010) 5782–5790.

[27] R.J.M. Pellenq, J.M. Caillol, A. Delville, Electrostatic Attraction between Two Charged Surfaces: A (N,V,T) Monte Carlo Simulation, J. Phys. Chem. B, 101 (1997) 8584–8594.

[28] A. Meleshyn, C. Bunnenberg, Swelling of Na/Mg-montmorillonites and hydration of interlayer cations: a Monte Carlo study, J. Chem. Phys., 123 (2005) 074706.

[29] P. Boulet, P.V. Coveney, S. Stackhouse, Simulation of hydrated Li^+, Na^+, K^+-montmorillonite/polymer nanocomposites using large-scale molecular dynamics, Chem. Phys. Lett., 389 (2004) 261–267.
[30] A. Cadene, B. Rotenberg, S. Durand-Vidal, J.C. Badot, P. Turq, Dielectric spectroscopy as a probe for dynamic properties of compacted smectites, Phys. Chem. Earth, 31 (2006) 505–510.
[31] S. Paumier, A. Pantet, P. Monnet, The effect of mineralogical and cationic heterogeneities on rheological properties of suspensions with Li-smectites, extracted from Volclay MX80, Adv. Colloid Interface Sci., 141 (2008) 66–75.
[32] I. Shainberg, A. Caiserman, Studies on Na/Ca montmorillonite systems. II. The hydraulic conductivity, Soil Sci., 111 (1971) 276.
[33] H.A. Velasco-Molina, A.R. Swoboda, C.L. Godfrey, Dispersion of soils of different mineralogy in relation to sodium adsorption ratio and electrolyte concentration, Soil Sci., 111 (1971) 282–287.
[34] H. Frenkel, J.O. Goertzen, J.D. Rhoades, Effects of clay type and content, exchangeable sodium percentage and electrolyte concentration on clay dispersion and soil hydraulic conductivity, Soil Sci. Soc. Am. J., 42 (1978) 32–39.
[35] J.D. Oster, I. Shainberg, J.D. Wood, Flocculation value and gel structure of Na/Ca montmorillonite and illite suspension, Soil Sci. Soc. Am. J., 44 (1980) 955–959.
[36] L.L. Schramm, J.C.T. Kwak, Influence of exchangeable cation composition on the size and shape of montmorillonite particles in dilute suspension, Clays Clay Miner., 30 (1982) 40–48.
[37] R. Keren, Effect of clay charge density and adsorbed ions on the rheology of montmorillonite suspension, Soil Sci. Soc. Am. J., 53 (1989) 25–29.
[38] W.R. Whalley, C.E. Mullins, Effect of saturating cation on tactoid size distribution in bentonite suspensions, Clay Miner., 26 (1991) 11–17.
[39] C. Malfoy, A. Pantet, P. Monnet, D. Righi, Effects of the nature of the exchangeable cation and clay concentration on the rheological properties of smectite suspensions, Clays Clay Miner., 51 (2003) 656–663.
[40] R. Pusch, J. Schomburg, Impact of microstructure on the hydraulic conductivity of undisturbed and artificially prepared smectitic clay, Eng. Geol., 54 (1999) 167–172.
[41] H. Masuda, D.R. Peacor, H. Dong, Transmission electron microscopy study of conversion of smectite to illite in mudstones of the Nankai Trough: contrast with coeval bentonites, Clays Clay Miner., 49 (2001) 109–118.
[42] G.E. Christidis, Formation and growth of smectites in bentonites: a case study from Kimolos Island, Aegean, Greece, Clays Clay Miner., 49 (2001) 204–215.
[43] J. Liu, I. Neretnieks, Physical and Chemical Stability of the Bentonite Buffer, Royal Institute of Technology, Sweden, 2006.
[44] Y. Yukselen, A. Kaya, Comparison of methods for determining specific surface area of soils, J. Geotech. Geoenviron. Eng., 132 (2006) 931–936.
[45] K.S.W. Sing, D.H. Everett, R.A.W. Haul, L. Moscou, R.A. Pierotti, J. Rouquerol, T. Siemieniewska, Reporting physisorption data for gas/solid systems with special reference to the determination of surface area and porosity (Recommendations 1984), Pure Appl. Chem., 57 (1985) 603–619.
[46] G.J. Churchman, C.M. Burke, Properties of subsoils in relation to various measures of surface area and moisture contents, J. Soil Sci., 42 (1991) 463–478.
[47] F. Salles, J.M. Douillard, O. Bildstein, S. El Ghazi, B. Prelot, J. Zajac, H. Van Damme, Diffusion of interlayer cations in swelling clays as a function of water content: case of montmorillonites saturated with alkali cations, J. Phys. Chem., C, 119 (2015) 10370–10378.
[48] N.W. Ockwig, R.T. Cygan, L.J. Criscenti, T.M. Nenoff, Molecular dynamics studies of nanoconfined water in clinoptilolite and heulandite zeolites, Phys. Chem. Chem. Phys., 10 (2008) 800–807.
[49] P. Clausen, W. Andreoni, A. Curioni, E. Hughes, C.J.G. Plummer, Water adsorption at a sodium smectite clay surface: an ab initio study of the first stage, J. Phys. Chem. C, 113 (2009) 15218–15225.